Modeling Wave-Enhanced Turbulence in the Ocean Surface Layer

PETER D. CRAIG

CSIRO Division of Oceanography, Hobart, Tasmania, Australia

MICHAEL L. BANNER

School of Mathematics, University of New South Wales, Kensington, New South Wales, Australia

(Manuscript received 6 October 1993, in final form 13 May 1994)

ABSTRACT

Until recently, measurements below the ocean surface have tended to confirm "law of the wall" behavior, in which the velocity profile is logarithmic, and energy dissipation decays inversely with depth. Recent measurements, however, show a sublayer, within meters of the surface, in which turbulence is enhanced by the action of surface waves. In this layer, dissipation appears to decay with inverse depth raised to a power estimated between 3 and 4.6. The present study shows that a conventional model, employing a "level 2½" turbulence closure scheme, predicts near-surface dissipation decaying as inverse depth to the power 3.4. The model shows agreement in detail with measured profiles of dissipation. This is despite the fact that empirical constants in the model are determined for situations very different from this near-surface application. The action of breaking waves is modeled by a turbulent kinetic energy input at the surface. In the wave-enhanced layer, the downward flux of turbulent kinetic energy balances its dissipation. The model produces analytic descriptions for the depth of the layer, and for profiles of velocity, turbulent kinetic energy, and dissipation. The surface roughness length (in the water) is a critical parameter in the solutions. There are indications of a relationship between the roughness length and surface wave parameters, such as the amplitude or inverse wavenumber. Roughness lengths at least up to 1 m appear to be feasible.

1. Introduction

At the ocean surface, momentum from the wind transfers to the water, driving the ocean's current systems. The momentum enters first the surface wave field and is transmitted to the surface current field mainly by wave breaking (e.g., Phillips 1977b). There is an attendant enhancement of turbulent kinetic energy close to the sea surface (e.g., Drennan et al. 1992); this turbulence is responsible for mixing the momentum down through the water, thus determining the shape of the near-surface current profile. The current profile in turn controls, for example, the movement of buoyant material such as fish larvae and contaminants and, from a more pragmatic perspective, determines the overturning moment on offshore structures such as oil platforms. However, measurement of currents, and other parameters, in the wave-affected layer is clearly difficult. Without measurement, models of the near-surface dynamics are, at best, tentative.

The classic model of wind-driven currents in the (rotating) ocean is that due to Ekman (1905). His solution assumes a constant eddy viscosity and predicts currents that decay exponentially with depth away from the surface. The constant eddy-viscosity model predicts a similar exponential boundary layer near the seabed. In the bottom boundary layer, measurements are more straightforward and, at least within a meter or so of the boundary, do not support the concept of exponential structure. Here, the widely accepted current profile is logarithmic (e.g., Gill 1982).

The concept of the logarithmic bottom boundary layer was originally based on laboratory tank observations. It is consistent with an eddy viscosity that varies linearly with distance above the boundary (e.g., Prandtl 1952). Such an eddy viscosity can be justified by mixing length arguments: the mixing length itself is assumed to increase linearly as

$$l = \kappa(|z| + z_0), \tag{1}$$

where κ is von Kármán's constant ($\sim$0.4), z is the vertical distance from the boundary, and z_0 is the "roughness length," representing the minimum scale of the turbulence. The eddy viscosity then has the form

$$A = \kappa u_*(|z| + z_0), \tag{2}$$

where u_* is the friction velocity (the square root of the shear stress per unit mass). In the boundary layer, the shear stress is constant, and the velocity profile is given, to within an additive constant, by

Corresponding author address: Dr. Peter D. Craig, CSIRO Division of Oceanography, GPO Box 1538, Hobart, Tasmania 7001, Australia.

$$u = \frac{u_*}{\kappa} \log(|z| + z_0). \quad (3)$$

By dimensional arguments, dissipation due to turbulent motion (ϵ) scales as the cube of the turbulent velocity (q) divided by the length scale l (e.g., Batchelor 1953). That is,

$$\epsilon = \frac{q^3}{Bl}, \quad (4)$$

where B is a constant of proportionality. In the boundary layer, q may be assumed to scale as u_*. Thus, in a constant stress layer, ϵ decreases inversely with the distance from the seabed. In boundary-layer studies, a region characterized by constant stress and a logarithmic velocity profile is commonly referred to as a "wall layer." Measurements of dissipation showing inverse proportionality with depth are regarded as evidence, if not proof, of "the law of the wall."

In environmental modeling, a linear eddy viscosity (2) and logarithmic velocity profile (3) have been accepted for many years as a description of the bottom boundary layer, both in the atmosphere (e.g., Ellison 1956) and ocean (e.g., Bowden et al. 1959). For ocean models that do not resolve the bottom boundary layer, the common quadratic and linear drag laws represent approximate conditions immediately at the top of the log layer. For the ocean surface, where observations are less reliable, the assumption of a log layer does not have such a long tradition (e.g., Madsen 1977). (See also Jenter and Madsen 1989, and Craig et al. 1993 for discussions of the modeling implications of log layers at both top and bottom boundaries.) There are now, however, a number of observations that appear to confirm the presence of such a surface layer. Among the more frequently quoted reports are those of Shemdin (1972, 1973) and Wu (1975) in tanks, Churchill and Csanady (1983) and Csanady (1984) in lakes, and Richman et al. (1987) in the ocean. We also note, in this context, observations by Jones (1985) that indicate log-layer structure to within five wave amplitudes of the surface, at winds of up to 15 m s^{-1} in Bass Strait.

The complication at the ocean surface, relative to the ocean floor, is surface waves, which have the potential to modify the dynamics in at least three different ways. The first, and best understood, is through Stokes drift (e.g., Phillips 1977a, section 3.3). Of the measurements cited in the previous paragraph, all but the final two sets were based on observation of drifters and will therefore be affected by Stokes drift. Bye (1988) suggests that the current profile for Stokes drift is also likely to be logarithmic. In this case, a logarithmic velocity profile may not necessarily indicate law-of-the-wall behavior.

The second influence of waves is mentioned for completeness. Waves that are not perfectly irrotational will generate a Reynolds stress on the mean motion (e.g., Phillips 1977a, section 3.4). Cheung and Street (1988) demonstrated and discussed this effect in their Case II experiment with wind-ruffled, mechanically generated waves in a tank. The resultant mean current profile (this time measured in an Eulerian frame) was again logarithmic, but with κ in (3) taking an apparently larger value than 0.4.

Cheung and Street (1988) briefly reviewed laboratory experiments and some field measurements set up to examine the influence of wind waves. They noted that most near-surface measurements tend to show agreement with the law of the wall, but with occasional evidence of excess downward momentum fluxes due to the presence of surface waves. Their own Case I experiment, with purely wind-driven waves, again confirmed the logarithmic velocity profile, but again indicated increased values of κ, this time with increasing wind speed and wave height.

The third influence of surface waves is the focus of the present paper. As waves begin to break, they release turbulent kinetic energy that is available to be mixed down into the surface layer. Recent innovative field techniques have allowed measurement well into the (breaking) wave-affected surface layer of lakes and the ocean. Kitaigorodskii et al. (1983) reported measurements using "drag spheres" mounted on a tower in Lake Ontario. These showed a region of enhanced turbulence down to about 10 times the wave amplitude, with "law-of-the-wall" behavior below that. Thorpe (1984) reported similar conclusions based on interpretation of acoustic reflections from bubbles in Loch Ness. Thorpe (1992) reiterated these observations, suggesting a wave-affected layer of depth approximately 0.2 of the surface wavelength. An elaborate, but foreshortened, experiment conducted by Osborn et al. (1992) used upward-looking acoustic equipment and shear probes mounted on a submarine in the Pacific Ocean. Their short records again show qualitative behavior consistent with the results of Thorpe (1984) and Kitaigorodskii et al. (1983).

Below the wave-enhanced zone, energy dissipation measurements (e.g., Osborn et al. 1992) and current measurements (e.g., Richman et al. 1987) show quantitative agreement with the law of the wall. For the wave zone, there are few fully quantitative results. From vertical-profiler measurements, however, Gargett (1989) inferred a dissipation rate decaying as the inverse fourth power of distance below the surface, substantially faster than the first-power decay predicted by the law of the wall. Further work on the Lake Ontario tower data (Drennan et al. 1992; Agrawal et al. 1992) has also provided quantitative results. Drennan et al. (1992) note that their dissipation rates also appear to decay with a power law close to -4 (in fact, in the range -3.0 to -4.6).

Anis and Moum (1992) present a very well-defined profile of dissipation, measured in the equatorial Pacific with a free-falling "Rapid-Sampling Vertical Profiler." Their profile again shows strong intensification of dis-

sipation, extending down to a depth of about 25 m, under winds of around 8 m s^{-1}. Plotted in log–log coordinates (not done in their paper), the data again exhibit power-law decay, with an exponent close to -3.

Drennan et al. (1992) compared their results with those from grid-stirring experiments conducted, for example, by Thompson and Turner (1975) and Hopfinger and Toly (1976). These experiments were an attempt to understand mixed-layer dynamics: mixing of stratified water in a tank is induced by oscillating a solid grid just below the surface of the water. Thompson and Turner (1975) suggested that the grid oscillation may be a reasonable analogy for breaking surface waves. Both sets of experiments appear to show turbulent velocities decaying as z^{-1}, that is, inversely with depth below the grid. By (4), this turbulence structure implies energy dissipation decaying as z^{-4}. In other words, recent measurements of wave-enhanced turbulence and earlier experiments designed to simulate the same dynamics appear to give similar behavior.

As noted by Cheung and Street (1988), many tank and lake observations of logarithmic velocity profiles have also revealed a sublayer, between the surface and the log layer, in which the velocity varies linearly with depth. We shall show in the present study that velocity variation as z (to be contrasted with the *turbulent* velocity variation of z^{-1}) is also consistent with dissipation of z^{-4}. The sublayer may thus be indicative of the appearance of whitecapping, as suggested by Csanady (1984). Bye (1988) has demonstrated that a linear-velocity layer may also occur in Stoke's drift, but the typical thickness of such a layer (for $u_* \sim 0.01$ m s^{-1}) is much less than 0.01 m.

Thompson and Turner (1975) derived support for the power-law behavior of the energy dissipation from a very simple model of the turbulent kinetic energy balance. The actual value of the power was derived empirically from the data. [For future reference, we note that their empirical constant κ in (1) takes a value smaller than von Kármán's, in contrast with the conclusion of Cheung and Street (1988).] As discussed in more detail in the following section, the Thompson and Turner model may be regarded as a forerunner of more complicated formulations, based on the turbulent kinetic energy equation, to assess the influence of breaking waves on the mean near-surface currents.

Another form of model (e.g., Jenkins 1986, 1987; Weber 1983; and Weber and Melson 1993a) incorporates both wave and current dynamics, allowing explicit representation of the Reynolds stresses due to the wave motion. These models assume an algebraic formulation for the (nonwave) eddy viscosity and do not specifically simulate the effect of wave breaking on the turbulence. Weber and Melson (1993b), however, have recently experimented with a parameterization of the momentum transfer from breaking waves to the mean motion for inclusion in such models. Another approach is the adoption of eddy viscosity formulations that attempt to account for the action of breaking surface waves. Thus, Weber (1981, using the formulation of Kitaigorodskii, 1961), and Davies (e.g., 1985, 1986, 1987) have tested eddy viscosities specified as a function of the wind and wave conditions. Interestingly, Jenkins (1987) specified an eddy viscosity according to (2) to within 10 wave amplitudes of the surface [based on Thorpe's (1984) results] but then constant over the surface layer. A z^{-4} dissipation implies, by (4), that u_* varies as z^{-1}, which in turn by (2) implies that the eddy viscosity is indeed constant in the wave-affected zone.

In a model that includes solution of (some form of) the turbulent kinetic energy equation, the eddy viscosity may be represented (on dimensional grounds) as the product of a turbulent velocity and length scale: this is, in fact, its form in (2). With the turbulent energy explicitly represented, the influence of breaking waves may be incorporated into a model as a source of energy at the surface. The energy input is usually assumed, again on dimensional grounds, to be proportional to the cube of the friction velocity. This is the approach to be adopted in the present study (see section 2).

In early examples of this approach (Kundu 1980; Klein and Coantic 1981), the inclusion of waves was almost incidental to a broader investigation of mixed layer deepening. Both studies led to the conclusion that, while velocity profiles within meters of the surface were affected by the inclusion of breaking waves, properties deeper in the water, and particularly the depth of the mixed layer, were unaffected. In a more theoretical study, Ly (1986, 1990) directed his attention specifically at the wave-affected zone. In this case, the wave layer was represented as a surface of both mean and turbulent energy discontinuity between the atmosphere and ocean. The discontinuity was expressed in proportionality to u_*^3 but not explicitly related to wave conditions nor given strong physical justification.

The turbulence closure schemes employed in each of the previous three studies are similar in concept but different in detail. In the present study, we adopt the scheme attributed to Mellor and Yamada (1974, 1982), based on the "Rotta" and "Kolmogorov" approximations to the equations for turbulent kinetic energy and Reynolds stresses. At the so-called level 2½, the scheme is highly empirical, requiring the assumption of a fundamental length scale and the specification of six numerical constants. The constants have been determined principally from observations of scenarios in which shear production of turbulence balances dissipation and in which the fundamental length scale can be safely specified as in (1) (Mellor and Yamada 1982). These are flows near solid boundaries in which the turbulence schemes asymptote to the law of the wall as the boundary is approached. However, the constants appear to be valid across a range of situations, including atmospheric boundary layer flows, penetrative convection and ocean mixed layer establishment

(e.g., Mellor and Yamada 1982; Rodi 1987; Chen et al. 1988; Wang et al. 1990).

We show in the present paper that the level-2½ scheme appears also to give reasonable results, given the present state of knowledge, in the wave-affected surface layer of the ocean. This is an unexpected result since the empirical constants are determined for a quite different dynamical regime. In the presence of breaking waves, shear production and dissipation of turbulence no longer balance, and the law of the wall no longer applies. For well-mixed water, as the surface layer will be, the level-2½ closure scheme requires only three empirical constants. These three appear to be consistent with recent observations of surface dynamics.

2. The model

We will work with a one-dimensional ocean model, equivalent to that described by Ekman (1905). The momentum equations are expressed in terms of the two horizontal velocity components u and v as

$$\frac{\partial u}{\partial t} - \frac{\partial}{\partial z}\left(A\frac{\partial u}{\partial z}\right) = fv \tag{5}$$

and

$$\frac{\partial v}{\partial t} - \frac{\partial}{\partial z}\left(A\frac{\partial v}{\partial z}\right) = -fu, \tag{6}$$

in which z is the vertical coordinate, measured positive upward from the seabed, $z = -H$, to the surface, $z = 0$. Time is represented by t, f is the Coriolis parameter, and A is the eddy viscosity. As foreshadowed in the previous section, A is to be determined with a level-2½ turbulence scheme (Mellor and Yamada 1982). In this scheme, A is expressed as

$$A = lqS_M, \tag{7}$$

where $l(z)$ is the turbulent length scale, as before, and q, the turbulent velocity scale, is formally defined as the square root of twice the turbulent kinetic energy density b (i.e., $q^2 \equiv 2b$). The parameter S_M in (7) is generally expressed as an algebraic function of the Richardson number. For unstratified water, however, it is an empirical constant. The equation for the turbulent kinetic energy is

$$\frac{\partial b}{\partial t} - \frac{\partial}{\partial z}\left(lqS_q\frac{\partial b}{\partial z}\right) = lqS_M\left(\left(\frac{\partial u}{\partial z}\right)^2 + \left(\frac{\partial v}{\partial z}\right)^2\right) - \frac{2qb}{Bl}, \tag{8}$$

in which S_q and B are also empirical constants. [Note that q and b in (8) in reality represent the same variable. The distinction is maintained for convenience.] In (8), the first term is the time rate of change of the energy, the next term represents its vertical diffusion, the first term on the right-hand side represents energy generation by velocity shear, and the final term is the dissipation, expressed exactly as in (4). The equation is clearly a highly approximate form of the turbulent kinetic energy balance. In a somewhat convoluted manner, for example, the energy is assumed to diffuse according to an eddy diffusion relationship, while the dissipation is based on (steady state) dimensional arguments presented, for example, by Batchelor (1953).

As an aside, we note that the full level-2½ scheme usually includes advective terms on the left-hand side, while the level-2 scheme neglects the left-hand side completely, assuming a strict balance between shear generation and dissipation of turbulence.

To finalize the set of equations, the last requirement is a specification of the turbulent length scale l. As noted by Mellor and Yamada (1982), the need for this length scale is perhaps a major weakness of the closure models. The simplest model for l is probably the mixed layer depth (e.g., Mellor and Durbin 1975), which in the case of unstratified water becomes the full water depth. The most complex model for l is possibly its specification using a differential equation similar to that for b (Mellor and Yamada 1982). There are numerous suggestions and ongoing discussion in the literature as to the best form for l (e.g., Blackadar 1962; Lobocki 1992). One feature common to most of the formulations for l is that they asymptote to the boundary layer form (1). As we shall see, the empirical constants in (8) are usually chosen so that the full turbulence model asymptotes to the law of the wall in this case. In the present formulation, we will assume that l behaves like (1) near both the top and bottom boundaries. The simplest way to do this is to specify a "bilinear" representation as follows:

$$\begin{aligned} l &= \kappa(z_0 - z), \quad -(H - z_0 + z_{0H})/2 \leqslant z \leqslant 0 \\ &= \kappa(H + z_{0H} + z), \quad -H \leqslant z \leqslant -(H - z_0 + z_{0H})/2 \end{aligned} \tag{9}$$

(e.g., Jenter and Madsen 1989; Craig et al. 1993), where z_0 and z_{0H} are roughness lengths for the top and bottom boundaries, respectively, both assumed invariant in time. The bottom roughness is a relatively well understood physical parameter (e.g., Jenter and Madsen 1989), and its significance for surface currents is documented (Craig et al. 1993). For notational simplicity, we set $z_{0H} = z_0$ in our formulae and fix $z_{0H} = 0.1$ m for specific calculations. Its role as a free parameter is henceforth ignored. For the surface roughness length z_0 a subsidiary model may have to be introduced but, for the present, it is assumed to be a known constant.

The full model, less boundary conditions, is now stated in Eqs. (5)–(9). The empirical constants to be specified are S_M, S_q, and B in the turbulence model itself and κ and z_0 in the length-scale model. According to Mellor and Yamada (1982), appropriate values (in their context) for the first three constants are

$$(S_M, S_q, B) = (0.39, 0.2, 16.6), \tag{10}$$

with von Kármán's constant $\kappa = 0.4$.

TABLE 1. Set of parameter values assumed for illustrative model solutions.

Parameter	Symbol	Value
Wind speed		9 m s^{-1}
Friction velocity	u_*	0.011 m s^{-1}
Wave energy factor	α	100
Surface roughness	z_0	0.1 m
Bottom roughness	z_{0H}	0.1 m
Water depth	H	100 m
Coriolis parameter	f	10^{-4} s^{-1}
Vertical discretization		41 points
Numerical time step		3600 s
von Kármán's constant	κ	0.4
Model constant	S_M	0.39
Model constant	S_q	0.2
Model constant	B	16.6

Boundary conditions for the velocity components are straightforward. At the water surface the stress is set equal to the wind stress, represented by the friction velocity u_*. Again following Ekman (1905), we specify a constant wind directed in the u direction, so that

$$A\frac{\partial u}{\partial z} = u_*^2 \quad \text{at} \quad z = 0 \tag{11}$$

$$A\frac{\partial v}{\partial z} = 0 \quad \text{at} \quad z = 0. \tag{12}$$

At the seabed, zero-slip requires that

$$u = v = 0, \quad z = -H. \tag{13}$$

The surface boundary condition on q allows us to introduce the influence of surface waves. Here, we specify an input of turbulent kinetic energy, assumed to result from breaking waves of all scales. However, while the level of the momentum flux from the atmosphere to the ocean is believed to be close to the total wind stress (e.g., Donelan 1979), as assumed in (11), there is apparently no such consensus in the literature on the turbulent kinetic energy flux. Typically, as noted in section 1, this quantity has been parameterized as proportional to the cube of the friction velocity in air or water, where the proportionality constant is not well known. In the absence of direct measurements, most authors leave the constant unresolved (e.g., Phillips 1985). According to Drennan et al. (1992), however, the kinematic turbulent kinetic energy input can be represented by $u_*^2 C_p$ where C_p is the phase speed of the peak of the *slope* spectrum of the surface displacement field.

More recently, Banner (personal communication) has proposed a model for estimating the contribution from air-flow separation over breaking waves to the atmospheric drag coefficient of the sea surface. This calculation produces a prediction of the spectral distribution of breaking wave–induced stress on the water column. The product of this stress with the intrinsic phase speed c of the breaking regions, integrated over the spectrum, in turn provides a prediction for the kinetic energy input as a function of u_* and sea state. The perceived merit of this approach is that the energy flux from the wind to the wave field very closely matches that transferred from the wave field to the water column by wave breaking; this criterion is not fulfilled by previous parameterizations. The additional kinetic energy input from tangential stresses appears to be of secondary importance, in view of the estimated shear stress magnitude and the relatively small associated (wind plus wave drift) velocity [estimated here as u_* from the work of Wu (1983)].

Surprisingly, it is found with this model that the turbulent kinetic energy flux is relatively insensitive to the sea state and is well approximated by αu_*^3, with $\alpha \sim 100$ for wave ages embracing very young wind seas to fully developed situations. The surface condition on q or b is thus stated as

$$lqS_q\frac{\partial b}{\partial z} = \alpha u_*^3 \quad \text{at} \quad z = 0. \tag{14}$$

The parameter α will be described as the "wave energy factor," assumed in model calculations to take a constant value of 100.

At the seabed, we assume zero flux of turbulent energy:

$$\frac{\partial b}{\partial z} = 0, \quad z = -H. \tag{15}$$

The implications of these equations, and particularly (14), are examined in the following sections.

Numerical solution

Numerical solution of the set of equations (5)–(15) is complicated by the need to resolve the surface and bottom boundary layers. This problem may be overcome by transforming the vertical coordinate according to

$$y = \int_0^z \frac{dz'}{l(z')}. \tag{16}$$

The transformation slightly simplifies the equations, in the sense that all instances of $l(z)\partial/\partial z$ are replaced by $\partial/\partial y$. Its major advantage, however, is that it expands the near-boundary regions, where l is small, relative to the interior part of the water column. Logarithmic velocity layers in z are replaced by layers in which the velocity varies linearly with y.

For the present paper, the set of equations (5)–(15) is expressed in terms of y rather than z, then solved by finite differences in both y and t. In space, the y domain is discretized into equally spaced intervals, and the differentials expressed in standard, second-order accurate, centrally differenced form. Each of b (or q), u, and v are collocated. In time, the equations are forward time-

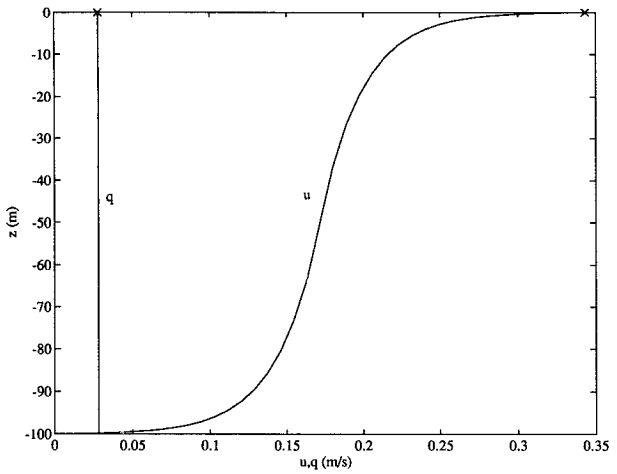

FIG. 1. Analytic solution for q and u as a function of depth for the nonrotating situation, with a strict balance between shear generation and dissipation in the turbulent kinetic energy equation.

stepped, and the vertical second derivatives solved implicitly. In (8), b in the dissipation term is also evaluated at the new time step. In each equation, variables not being integrated, including q, take their current values. This implicit time integration is very stable.

In the time integrations the forcing, specified through boundary conditions (11) and (14), is applied impulsively at $t = 0$. The velocity components were set to zero at $t = 0$. The surface value of q was set at $t = 0$ to the analytic surface solution for a shear production–dissipation balance (see section 3), with deeper values set to $1/100$ of the surface value. The preset surface value improved the stability of the model.

For examples to be presented in the following sections, assumed parameter values are listed in Table 1.

3. Shear production balancing dissipation

In this section, we will look in some detail at the "usual" boundary-layer balance between the shear production and dissipation of turbulent kinetic energy. This is the situation that leads to classical logarithmic boundary layers. Although the numerical equations are time stepped, we will concentrate in this paper on the steady solutions. We comment briefly on time scales required to establish steadiness at the end of the present section.

The relevant steady equations are (5) and (6), with the $\partial/\partial t$ terms eliminated, and (8), with the left-hand side replaced by zero. The two terms on the right-hand side represent the required shear production and dissipation, respectively.

The surface boundary condition is (11), which, by (8), immediately gives

$$q = u_*\left(\frac{B}{S_M}\right)^{1/4} \quad \text{at} \quad z = 0. \tag{17}$$

With values for B and S_M given in (10),

$$\left(\frac{B}{S_M}\right)^{1/4} = 2.55. \tag{18}$$

Now, by (7) and (9),

$$A = (S_M^3 B)^{1/4}\kappa u_* z_0 = 1.00\kappa u_* z_0 \quad \text{at} \quad z = 0, \tag{19}$$

in agreement with (2). Of course, the constants are chosen to ensure this agreement (Mellor and Yamada 1982).

If, for the moment, we ignore rotation so that the right-hand side of (5) is zero, then $v = 0$ and, by (8), q is constant, taking the value given by (17) throughout the water column; u can be determined analytically as

$$u = \begin{cases} \dfrac{u_*}{\kappa(S_M^3 B)^{1/4}} \log \dfrac{\left(z_0 + \dfrac{H}{2}\right)^2}{z_0(z_0 - z)}, & -\dfrac{H}{2} \leqslant z \leqslant 0 \\ \dfrac{u_*}{\kappa(S_M^3 B)^{1/4}} \log \dfrac{z_0 + H + z}{z_0}, & -H \leqslant z \leqslant -\dfrac{H}{2}. \end{cases} \tag{20}$$

The logarithmic form of u at both top and bottom boundaries is explicit in this solution, which is plotted in Fig. 1. The analytic result provides a test for the numerical solution, and the two are in fact indistinguishable on the scale of the figure.

With rotation reintroduced, the solution is no longer so amenable to analytic solution. Steady numerical solutions for u, v, and q are shown in Fig. 2. Very close to the top and bottom boundaries, there are layers in which q and v are strictly constant and u varies logarithmically. The velocity now spirals to the right with

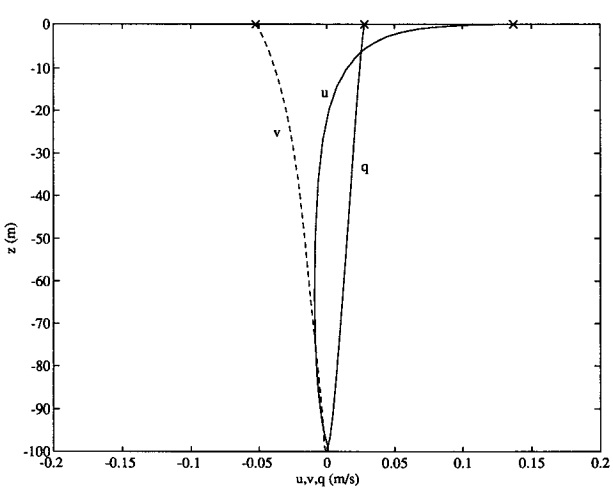

FIG. 2. Profiles of q and u (solid lines) and v (dashed line) for the case of a balance between the shear generation and dissipation of turbulent kinetic energy. Surface values are marked with an "X" for clarity.

depth (for positive f), in classic Ekman fashion. Surface velocities are considerably reduced, but the surface value of q is unchanged from that in the irrotational situation. For future reference, we note that the velocity profile in the log layer may be expressed analytically as

$$u = U - \frac{u_*}{\kappa(S_M^3 B)^{1/4}} \log(z_0 - z), \qquad (21)$$

in which U is an additive constant velocity that must be determined from the full solution.

By (19), the eddy viscosity ($=lqS_M$) may be scaled as $\kappa u_*|z|$, the form of the viscosity assumed by Craig et al. (1993), so that their conclusions are valid in the present context. In particular, the dynamical vertical length scale is approximately $\kappa u_*/f$ (in fact, an overestimate since now qS_M decreases through the water from a maximum value of u_* at the surface). The log-layer depth will be small relative to $\kappa u_*/f$, and the amount of turning and decay in magnitude of the currents with depth will increase if $\kappa u_*/f$ decreases relative to the water depth. For water depths greater than $\kappa u_*/f$ the solutions are not sensitive to boundary conditions at the bottom. In Fig. 2, $\kappa u_*/f$ takes a value of 44 m. As an indication of the depth of the log layer in this case, the u component of the velocity agrees with the logarithmic solution (21) to within 0.2% at 0.4 m, and 7% at 4.4 m depth.

At this stage, we can make a passing comment about timescales. If the eddy viscosity in (5) or (6) is again represented by $\kappa u_*|z|$, then the spinup time estimated from the left-hand side of either equation (using either analogy with the constant viscosity case or a Bessel function solution) is of the order $\pi H/2\kappa u_*$. For the parameters from Table 1, this scale is approximately 10 hours. Thus, the steady solutions of Figs. 1 and 2 are established on timescales that are the same or shorter than those associated with propagating weather patterns. However, a long-duration (many days) inertial oscillation is set up in the velocities (but not in the solution for q). The inertial oscillation is damped from the bottom boundary, a very much slower process, since the value of q, and thus the eddy viscosity, is much smaller near the bottom (rather than the top) boundary (see Fig. 2).

4. Diffusion balancing dissipation

The situation of more importance in the present context is that in which turbulent kinetic energy is produced at the surface according to (14). To examine this phenomenon in more detail, we will again simplify the equations, once more considering the steady state, but now eliminating the shear production term from (8). The turbulent kinetic energy equation now represents a balance between the downward diffusion of energy injected at the surface and its dissipation.

Equation (8) can now be re-expressed as

$$\frac{1}{3} S_q \kappa^2 B \frac{\partial}{\partial z}\left((z_0 - z)\frac{\partial q^3}{\partial z}\right) = \frac{q^3}{z_0 - z} \qquad (22)$$

in the upper half of the water column, with an equivalent form in the lower half. Equation (22) is very similar to the energy balance invoked by Thompson and Turner (1975). The right-hand side is identical, being based on the same model for dissipation. In their case, however, the left-hand side contained only a first derivative in z, being a representation of the vertical advection of turbulent energy. The solution to (22) is

$$q^3 = \begin{cases} c_+(z_0 - z)^n + c_-(z_0 - z)^{-n}, & -\dfrac{H}{2} \leqslant z \leqslant 0 \\ d_+(z_0 + H + z)^n + d_-(z_0 + H + z)^{-n}, & -H \leqslant z \leqslant -\dfrac{H}{2}, \end{cases} \qquad (23)$$

where

$$n = \left(\frac{3}{S_q \kappa^2 B}\right)^{1/2} = 2.4 \qquad (24)$$

and c_+, c_-, d_+, and d_- are constants to be determined (analytically) from boundary conditions (14) and (15) and the continuity of q and $\partial q/\partial z$ at $z = -H/2$.

The c_- term in (23) represents decay away from the surface, and we expect this to dominate the c_+ term, which represents reflected energy from the bottom. (For the selected model parameters, c_+ is, in fact, zero to within numerical accuracy.) Near the surface then, q is described by

$$q = C(z_0 - z)^{-n/3}, \qquad (25)$$

where $C = c_-^{1/3}$. With constants evaluated from (10), the exponent $n/3$ in (25) takes a value 0.8. According to (4), the dissipation therefore varies as

$$\epsilon = \frac{C^3(z_0 - z)^{-n-1}}{\kappa B}, \qquad (26)$$

that is, as z to the power of -3.4. Significantly, this power is close to the values reported in studies in section 1. It lies well within the range -3.0 to -4.6 reported by Drennan et al. (1992) and is similar to the -3 power of the Anis and Moum (1992) data.

If we assume that (25) is the solution for q (i.e., that c_+ is exactly zero), then C can be determined from boundary condition (14) to give, in the upper half of the water column,

$$q = u_* \alpha^{1/3}\left(\frac{3B}{S_q}\right)^{1/6}\left(\frac{z_0}{z_0 - z}\right)^{n/3}. \qquad (27)$$

With q expressed in this form, it is clear that the vertical length scale for the decay of both q and ϵ is z_0 so that

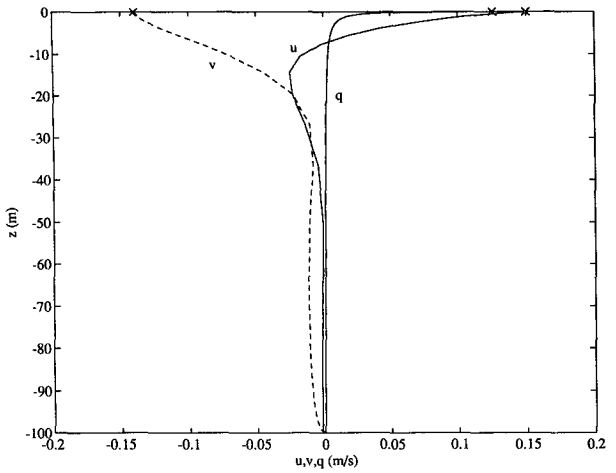

FIG. 3. Profiles of q, u, and v for the case of a strict balance between the downward diffusion of turbulent kinetic energy from a surface source and its dissipation.

(27) is indeed likely to be a very accurate approximation of (23). There will be effectively no turbulent kinetic energy reaching even middepth if the water depth is large compared with z_0. It is also clear from (27) that q is not a strong function of the wave energy factor α, varying only as its 1/3 power. [As noted in section 2, we have chosen α to be constant, while Drennan et al. (1992) equate it to the wave age.] The constant factor in (27) evaluates, by (10), to

$$\left(\frac{3B}{S_q}\right)^{1/6} = 2.51. \tag{28}$$

The multiplicative constants in (17) and (27) agree to within 2%. We will denote their ratio by

$$r = \left(\frac{B}{S_M}\right)^{1/4}\left(\frac{S_q}{3B}\right)^{1/6}, \tag{29}$$

which takes a value of 1.0.

In the constant stress layer near the surface [in which the right-hand side of (5) may be neglected], u will vary with depth as the positive power $n/3$. Specifically,

$$u = U - 3r^4 u_* \alpha^{-1/3}\left(\frac{z_0 - z}{z_0}\right)^{n/3}, \tag{30}$$

in which U is an additive constant similar to, but taking a different value from that in (21).

The solution for q [from Eq. (23)], using the set of parameters from Table 1, is shown in Fig. 3, together with the numerical solution for u and v. (Again, the numerical and analytic solutions for q are virtually indistinguishable on the scale of the figure.) With q of the form (27), the eddy viscosity varies vertically as $(z_0 - z)^{1-n/3}$. That is, A is close to constant with depth so that the profiles for u and v in Fig. 3 closely resemble the classic Ekman (1905) solution. Obvious manifestations of this resemblance are the near linearity of the velocity (30) in the constant stress layer and the near equality in magnitude of u and v at the water surface.

5. The full model

Figure 4 shows the steady solutions for q, u, and v for the full model, including the effects of both diffusion and shear generation of turbulent kinetic energy. The solution for q is replotted on an expanded vertical scale in Fig. 5a, highlighting the surface layer. The figure also shows the solutions from Figs. 2 and 3. It is immediately apparent from these curves that q follows the diffusion–dissipation model of section 4 in the near-surface layer but then changes, over a relatively small depth, to the shear-generation solution of section 3. For convenience, we will refer to the near-surface as "the wave-enhanced layer," and the deeper water as "the shear layer."

We can estimate the depth of the transition from the wave-enhanced to the shear layers as follows. In the diffusive near-surface region the solution for q is given by (27), while in the shear-dominated region it takes the constant value (17). Given that the multiplicative constants in the two formulae agree, the surface value of the diffusive q of (27) is bigger than the shear-generated q of (17) by a factor of $\alpha^{1/3}$. By equating (27) and (17), we get the depth at which the two are equal to be

$$z_t = z_0(1 - r^{-3/n}\alpha^{1/n}), \tag{31}$$

in which, by (24), the exponent $1/n$ has a value of 0.4. In other words, the transition depth is proportional to the roughness length and weakly dependent on the factor α. For $\alpha = 100$ used in Fig. 5, $z_t = -6z_0 = -0.6$ m. The actual crossover point for the shear and diffusive curves in Fig. 5a is almost exactly 0.6 m, while the full transition occurs between 0.2 and 2 m.

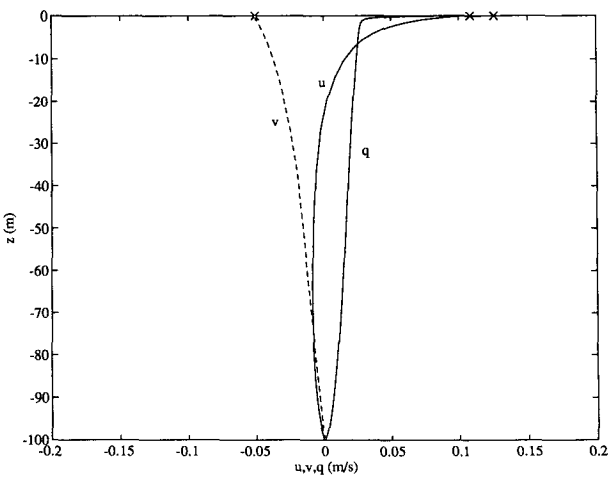

FIG. 4. Profiles of q, u, and v for the full model, with a surface flux of turbulent kinetic energy, shear generation, and dissipation.

The full (steady) solution for u is similarly replotted in Fig. 5b, again with the solutions from sections 3 and 4. As is to be expected from Fig. 5a, there is a transition from diffusion-dominated to shear-dominated behavior near z_t. The horizontal displacement of the diffusive-u curve in Fig. 5 is simply due to the change in conditions below z_t, corresponding to a different additive constant in (30).

Below the transition depth, the velocity profile is the same as that for the shear generation–dissipation balance. In the surface layer, the influence of the enhanced turbulence is to reduce the velocities below those anticipated for strictly log-layer behavior. We can estimate the magnitude of the velocity deficit as follows. We assume the transition takes place within the constant shear layer and set the velocities (21) and (30) equal at $z = z_t$. The velocity deficit in the surface layer is now given by

$$\delta u = -\frac{u_*}{\kappa(S_M^3 B)^{1/4}} \log\left(\frac{z_0 - z}{z_0 - z_t}\right) + 3r^4 u_* \alpha^{-1/3} \times \left[\left(\frac{z_0 - z}{z_0}\right)^{n/3} - \left(\frac{z_0 - z_t}{z_0}\right)^{n/3}\right]. \quad (32)$$

For parameter values relevant to Fig. 5, (32) gives a reduction in surface velocity, due to the presence of the wave-enhanced layer, of 0.024 m s^{-1} compared with the exact value of 0.029 in the figure.

It is also straightforward to estimate the enhancement of dissipation due to the wave energy input. This simply requires integration of the dissipation, estimated from (17) and (27), from z_t to the surface. For (17), the integrated dissipation is given by

$$\int_{z_t}^{0} \epsilon dz = r^3 u_*^3 \log\alpha, \quad (33)$$

while for (27),

$$\int_{z_t}^{0} \epsilon dz = u_*^3(\alpha - 1), \quad (34)$$

which evaluate to 6×10^{-6} and 1.3×10^{-4} m^3 s^{-3}, respectively, for the parameters in Table 1. The near-surface dissipation due to the influence of waves dominates that due to shear in both the surface and deeper layers by a factor of about 20, which is independent of u_*.

The principal formulae of this section, those for the transition depth (31), the surface velocity deficit (32), and the wave-enhanced dissipation (34), are only accurate if the wave-enhanced layer is no deeper than the log layer, that is, $z_t \ll \kappa u_*/f$. In pictorial form, once the intersection of the diffusive and shear curves on Fig. 5a falls below the vertical part of the shear curve, the accuracy of the formulae will begin to decline.

As has already been noted, the roughness length z_0 defines the vertical scale for the wave-enhanced layer.

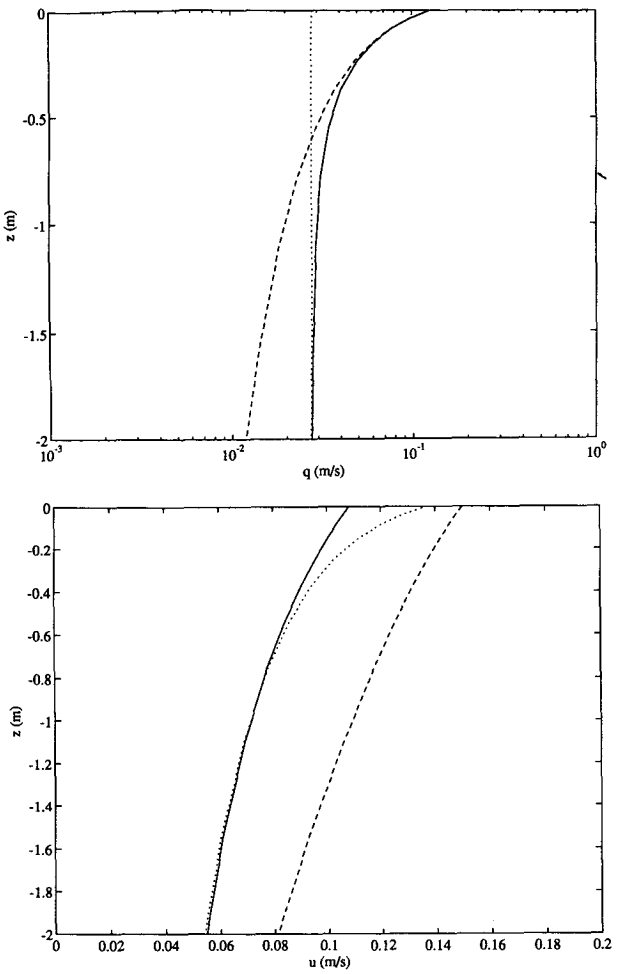

FIG. 5. Near-surface profiles of (a) q and (b) u, showing the full solution (solid line), the diffusion–dissipation balance (dashed line), and the shear–dissipation balance (dotted line).

This is apparent in the formulae for the turbulent kinetic energy (27), the velocity (30), and the layer depth (31). For a given u_* and α, however, the value of z_0 does not affect the surface value of q, the velocity deficit δu (although it does affect the absolute value of u), or the total energy dissipation in the surface layer.

The effects of changes in z_0 are demonstrated in Fig. 6, showing profiles of q and u for z_0 values of 0.1, 0.5, and 1.0 m. (In all cases, the bottom roughness was kept at 0.1 m.) Anticipated, and readily apparent, consequences of increasing z_0 are the deepening of the wave-enhanced layer, increases in subsurface turbulent energy, and reduction of near-surface velocities.

6. Comparison with data

The turbulence closure model appears to successfully reproduce two recently observed features of the influence of waves on subsurface dynamics: appropriate

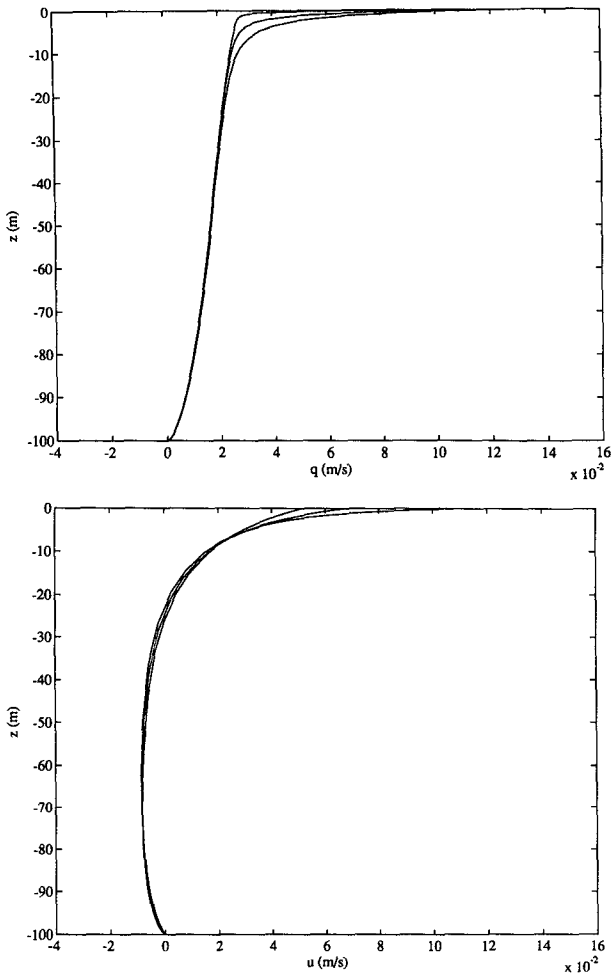

FIG. 6. Profiles of (a) q and (b) u for a roughness lengths of 0.1, 0.5, and 1.0 m. Curves near the surface move from right to left with increasing z_0 for q, but from left to right for u.

power-law behavior immediately below the surface and preservation of log-layer behavior deeper in the water. In this section, we pursue a more quantitative comparison of the model with published data. As we shall see, this comparison leads to questions about appropriate choices for the surface roughness length z_0.

On the basis of their Lake Ontario data, Drennan et al. (1992) postulated an empirical dissipation law in the surface layer given by

$$\epsilon = 1.84u_*^3\alpha k^{-3}(-z)^{-4}, \tag{35}$$

in which k is the wavenumber of the peak of the slope spectrum. This formula bears strong similarity to that derived from (27), that is,

$$\epsilon = 2.4u_*^3\alpha z_0^n(z_0 - z)^{-n-1}, \tag{36}$$

provided z_0 takes a value similar to k^{-1}. Both the algebraic form of the formulae and the empirical constant are in close agreement. In (35), α is specifically identified as the wave age, whereas, as discussed in section 2, we have preferred to keep it as a constant. For a u_* of 0.011 m s^{-1}, as used in examples in the present study, the wave age (the ratio of the phase speed of the steepest waves to u_*) is estimated (by the wave model of Banner, see section 2) to take values between 183 and 396, from young to old seas, with a corresponding k range of 1.86–0.46 m^{-1}.

As noted in section 1, and in particular by Cheung and Street (1988), many measurements showing logarithmic near-surface velocity profiles have also revealed a linear profile even closer to the surface. According to (30), in the wave-enhanced layer the velocity should vary as $z^{0.8}$, very close to linear. Interpolating their measured linear profiles to the surface, Churchill and Csanady (1983) and Csanady (1984) calculated an observed surface Reynolds number, defined by

$$\mathrm{Re} = \frac{30z_0u_*}{A} = \frac{30z_0(\partial u/\partial z)}{u_*} \quad \text{at} \quad z = 0. \tag{37}$$

The parameter Re appeared to be independent of both u_* and z_0, with values ranging between 17 and 27 but averaging about 22. For the theoretical logarithmic velocity profile (21)

$$\mathrm{Re} = \frac{30}{\kappa(S_M^3B)^{1/4}} = 75 \tag{38}$$

while, for a wave-enhanced "linear" profile (30),

$$\mathrm{Re} = 30nr^4\alpha^{-1/3} = 16. \tag{39}$$

Both solutions (38) and (39) are indeed independent of u_* and z_0, but the wave-enhanced solution gives a surface Reynolds number much more compatible with the observations. For the Stokes drift profile (Bye 1988), the surface Reynolds number takes a value of 86, of similar order to the log-profile value.

Some of the data on which (35) is based were published by Agrawal et al. (1992). Figure 7 shows a comparison between model results and the Agrawal et al. data, plotted in their coordinates, with ϵ nondimensionalized by $u_*^3/\kappa z$, and depth by u_*^2/g. While the data are for a range of conditions, the model results in Fig. 7 are for the parameter values listed in Table 1 (including a fixed u_* of 0.011 m s^{-1}) but for two z_0 values, 0.1 and 1.0 m. The resulting pair of solutions envelope most of the near-surface dissipation values. There are, however, some high values that are not accounted for by this set of parameters. The law-of-the-wall solution is shown as a dotted line on Fig. 7.

The Osborn et al. (1992) data, discussed in section 1, allow for similar comparison. Figure 8 shows model results, again for z_0 values of 0.1 and 1.0 m, plotted against data from the Osborn et al. Figs. 9b and 9d. In this case, the model was run with a u_* of 0.007 m s^{-1} (from their Table 1), and a water depth of 200 m. This water depth is much greater than the depth scale $\kappa u_*/f$, so the bottom conditions should not influence the

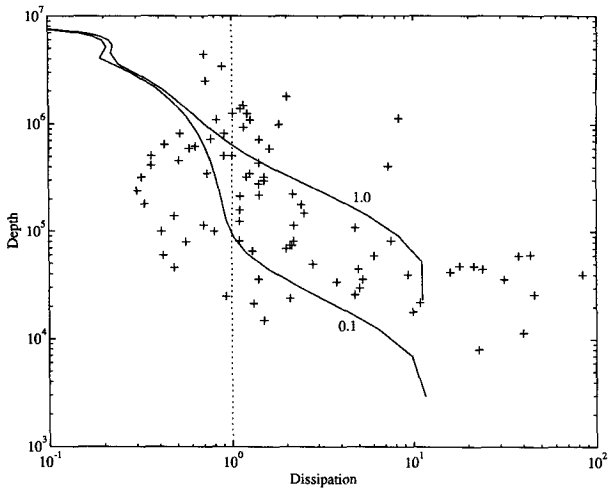

FIG. 7. Comparison of modeled dissipation profiles for $z_0 = 0.1$ and 1.0 m with data from Agrawal et al. (1992). Dissipation is nondimensionalized as $\epsilon\kappa z/u_*^3$, and depth as zg/u_*^2. The dotted line represents the conventional law-of-the-wall solution.

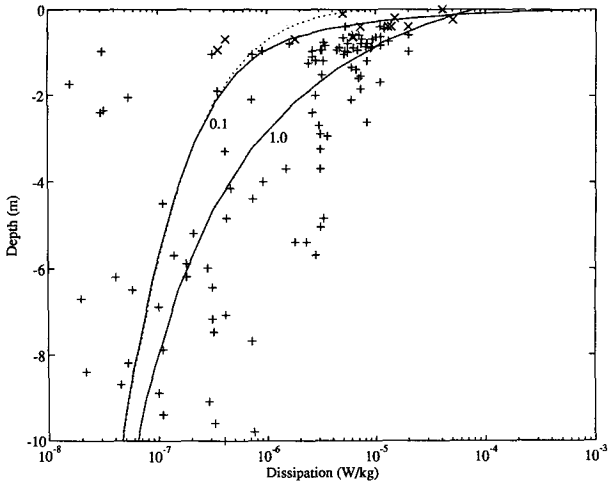

FIG. 8. Comparison of modeled dissipation profiles, for $z_0 = 0.1$ and 1.0 m, with data from Osborn et al. (1992). Data are from their figures 9b (+) and 9d (×). The dotted line represents the solution for a pure shear generation–dissipation balance.

solutions. Again, the two model curves appear to envelope the data points near the surface. There is perhaps some evidence of surface enhancement extending beyond the depth predicted by the model.

The data in Fig. 8 are from only two transects through the surface layer. The dissipation curve presented by Anis and Moum (1992) (see section 1) is an average of approximately 80 profiles collected throughout a single night. As we have already noted, the slope of their dissipation curve, −3, is very similar to the −3.4 predicted by (36). However, an attempt to fit the model to the data, using $u_* = 0.0087$ m s^{-1}, $f = 0.00002$ s^{-1}, and $H = 200$ m (again, greater than $\kappa u_*/f$), required a z_0 of 8 m to produce a reasonable fit (Fig. 9). This anomolously large value is probably indicative of failure of the model, but the Anis and Moum dataset, unlike others used here, was collected in the presence of swell. It is possible that swell may lead to dynamics, particularly the downward advection of smaller scale turbulence not represented in the model [Eq. (8)]. Vertical advection, deepening the wave-affected layer, could also result from Langmuir circulation.

We have, to this stage, avoided detailed discussion of the surface roughness z_0. The roughness of the sea surface as felt by the atmosphere is a relatively well-understood, but empirical, function of wind speed and wave age (e.g., Donelan et al. 1993). In the atmosphere, estimation of the roughness length is usually based on extrapolation of the logarithmic velocity profile to the sea surface. The roughness felt by the ocean, however, is not well known or understood, essentially because of the dearth of velocity measurements in the ocean surface layer. While many authors acknowledge the need for z_0 (e.g., Madsen 1977; Mellor and Yamada 1982; Jenter and Madsen 1989; Craig et al. 1993), most seem reluctant to commit themselves to a value. Madsen (1977), in fact, referred to the "rather unpleasant problem of estimating" z_0. He suggested an order of 10^{-3} m. Earlier, Shemdin (1972, 1973), on the basis of wind-tunnel experiments, suggested 10^{-4} m, similar to the atmospheric value.

Churchill and Csanady (1983) and Csanady (1984) applied the atmospheric approach to their sets of near-surface drifter data collected in lakes. The observations were taken under relatively light wind conditions (wind velocities at 3 m less than 5 m s^{-1}), with u_* estimates

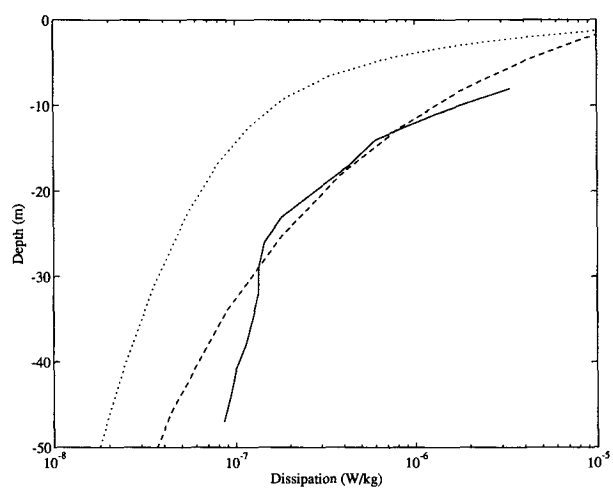

FIG. 9. Comparison of modeled dissipation profiles (discontinuous lines) with Anis and Moum (1992) data (solid line). The dotted and dashed lines are the modeled dissipation with $z_0 = 1$ and 8 m, respectively.

generally less than 0.01 m s^{-1}. Their estimates for z_0 lie in the range of 0.01–0.1 m (accounting for the fact that their roughness parameter, "r" in their notation, is 30 times z_0).

In the absence of other representations, the most popular approach to z_0 is probably adoption of the "Charnock (1955) formula,"

$$z_0 = \frac{au_*^2}{g}, \tag{40}$$

(in which a is a constant) justified by analogy with the atmosphere (e.g., Ly 1990). As noted in section 1, Bye (1988) interpreted near-surface log and linear velocity profiles strictly in terms of Stokes drift. On this basis, he proposed use of (40), with a of order 1400. For the Csanady data, this formula again leads to z_0 values around 0.01 m.

Observations of near-surface drifters are clearly not taken under conditions of strong whitecapping or wave breaking. From the present study, we are able to make tentative statements about z_0 under more severe conditions. As noted in section 1, Thorpe (1992) and others suggested that the wave-affected layer has a depth of order 10 times the wave amplitude. Equating this depth to the transition depth of (31) suggests that z_0 must then be of the same order as the wave amplitude. However, this statement raises questions about the appropriate wave amplitude to be used. While Thorpe's (1992) comment was based on the root-mean-square wave height, he has recently (Thorpe 1993) conjectured that high frequency waves, rather than the mean wave field, are the major source of energy input to the upper ocean. This conclusion also emerges from modeling by Banner (see section 2). In their grid-stirring experiments, Thompson and Turner (1975) equated z_0 to the stroke of the grid motion. This may have some analogy to the wave amplitude. We have noted above that comparison between the model and the Drennan et al. (1992) formula suggests z_0 to be of the order of the inverse wavenumber of the steepest waves. Comparisons with the Agrawal et al. (1992) and Osborn et al. (1992) data indicate values for z_0 between 0.1 and 1.0 m.

We note in passing that z_0 appears in most formulae in the previous two sections as a product with $\alpha^{1/n}$. Thus, changes in either of the two parameters will have similar consequences.

Determination of z_0 will no doubt receive increasing attention as more measurements near the sea surface become available. In reality, the adoption of the roughness length concept is an admission that our mixing length models fail very close to the surface. For the ocean, z_0 is no doubt a function, at least, of sea state, swell, and Langmuir circulation. In the longer term, we will hopefully develop a more dynamical, less empirical, basis for surface roughness lengths relevant to both the ocean and atmosphere.

7. Conclusions

The classical law of the wall description of the ocean surface layer predicts dissipation decaying as z^{-1} away from the surface. However, recent measurements (Gargett 1989; Drennan et al. 1992; Anis and Moum 1992) indicate much more rapid dissipation in the range z^{-3}–$z^{-4.6}$, presumably as a result of increased turbulence due to surface waves. This dissipation is similar to the z^{-4} behavior observed in earlier grid-stirring experiments (Thompson and Turner 1975; Hopfinger and Toly 1976). Model results presented in the present paper predict a decay rate of $z^{-3.4}$, well within the range of the observations. The predicted velocity profile associated with this dissipation varies linearly with depth, consistent with drifter measurements very close to the surface (e.g., Csanady, 1984).

The essential elements of the model are

1) a Prandtl-type (1952) mixing length specification;
2) a turbulent kinetic energy equation representing a balance between parameterized versions of diffusion, dissipation, and shear generation;
3) an eddy viscosity proportional to the mixing length and the turbulent kinetic energy; and
4) a surface turbulent kinetic energy input, due to the waves, set proportional to the cube of the friction velocity.

The three empirical constants (aside from von Kármán's constant) used in the model were given values recommended by Mellor and Yamada (1982). The model not only predicts the form of the dissipation but is able to reproduce reasonably well, given the data scatter, dissipation measurements recently published by Agrawal et al. (1992) and Osborn et al. (1992).

In the wave-enhanced layer, the model predicts dynamics that are a balance between the downward flux of turbulent kinetic energy from the surface and its dissipation. Beneath this layer, there is a relatively rapid transition to classical law-of-the-wall behavior, in which the shear generation of turbulent kinetic energy is balanced by dissipation. The dynamics of the shear-generation layer are almost unaffected by the presence of the wave-enhanced layer. For model studies in which the very near-surface dynamics are of no interest, there appears to be no need to include the surface injection and subsurface diffusion of the turbulent kinetic energy.

The model makes specific predictions for the dynamical variables in the surface layer. On the assumption that the wave-enhanced layer is shallower than the log layer (i.e., that the wave-enhanced layer depth is much smaller than $\kappa u_*/f$), these predictions can be expressed analytically as functions of the friction velocity, the surface roughness length, and the wave energy factor α. Specific formulae are (31) for the depth of the layer, (34) for the (integrated) dissipation in the layer, and (27), (30), and (36) for the profiles of tur-

bulent kinetic energy, velocity, and dissipation, respectively.

One tentative conclusion of the study is that the water-side sea surface roughness length is much greater than that for the atmosphere. Values at least up to 1 m seem feasible. There are indications that the roughness length is related to, and of similar magnitude to, a wave amplitude or an inverse wavenumber, such as that of the steepest waves.

We make no claim to have produced the definitive description of the near-surface dynamics of the ocean. However, our study has shown that this conventional and relatively simple model appears to do rather well in reproducing our present knowledge of the wave-affected zone. The model has produced predictions that may be useful benchmarks for further measurement programs. There is considerable scope for extending the model as more extensive and reliable data become available. Initially, this extension could focus on refining the empirical parameters before refinement of the parameterizations themselves. We reiterate from section 1, for example, conflicting comments about the value of κ by Cheung and Street (1988) and Thompson and Turner (1975). There is a priority requirement for realistic models of the sea surface roughness.

Acknowledgments. We wish to thank Professors Stewart Turner and Henry Charnock for their insight during the course of this study and Professor Stephen Thorpe for his careful comments on a draft of the manuscript.

REFERENCES

Agrawal, Y. C., E. A. Terray, M. A. Donelan, P. A. Hwang, A. J. Williams, W. Drennan, K. Kahm, and S. Kitaigorodskii, 1992: Enhanced dissipation of kinetic energy beneath breaking waves. *Nature,* **359,** 219–220.

Anis, A., and J. N. Moum, 1992: The superadiabatic surface layer of the ocean during convection. *J. Phys. Oceanogr.,* **22,** 1221–1227.

Batchelor, G. K., 1953: *The Theory of Homogeneous Turbulence.* Cambridge University Press, 197 pp.

Blackadar, A. K., 1962: The vertical distribution of wind and turbulent exchange in a neutral atmosphere. *J. Geophys. Res.,* **67,** 3095–3102.

Bowden, K. F., L. A. Fairbairn, and P. Hughes, 1959: The distribution of shearing stresses in a tidal current. *Geophys. J. Roy. Astron. Soc.,* **2,** 288–305.

Bye, J. A. T., 1988: The coupling of wave drift and wind velocity profiles. *J. Mar. Res.,* **46,** 457–472.

Charnock, H., 1955: Wind stress on a water surface. *Quart. J. Roy. Meteor. Soc.,* **81,** 639–640.

Chen, D., S. G. Horrigan, and D.-P. Wang, 1988: The late summer vertical nutrient mixing in Long Island Sound. *J. Mar. Res.,* **46,** 753–770.

Cheung, T. K., and R. L. Street, 1988: The turbulent layer in water at an air-water interface. *J. Fluid Mech.,* **194,** 133–151.

Churchill, J. H., and G. T. Csanady, 1983: Near-surface measurements of quasi-lagrangian velocities in open water. *J. Phys. Oceanogr.,* **13,** 1669–1680.

Craig, P. D., J. R. Hunter, and B. L. Johnston, 1993: The implications of linearly varying eddy viscosity for wind-driven current profiles. *Contin. Shelf Res.,* **13,** 1–24.

Csanady, G. T., 1984: The free surface turbulent shear layer. *J. Phys. Oceanogr.,* **14,** 402–411.

Davies, A. M., 1985: A three-dimensional model of wind induced flow in a sea region. *Progress in Oceanography,* Vol. 15, Pergamon Press, 71–128.

——, 1986: Application of a spectral model to the calculation of wind drift currents in an idealized stratified sea. *Contin. Shelf Res.,* **5,** 579–610.

——, 1987: On extracting current profiles from vertically integrated numerical models. *Coastal Eng.,* **11,** 445–477.

Donelan, M. A., 1979: On the fraction of wind momentum retained by waves. *Marine Forecasting, Marine Predictability and Modelling in Ocean Hydrodynamics,* J. C. J. Nihoul, Ed., Elsevier, 141–159.

——, F. W. Dobson, S. D. Smith, and R. J. Anderson, 1993: On the dependence of sea surface roughness on wave development. *J. Phys. Oceanogr.,* **23,** 2143–2149.

Drennan, W. M., K. K. Kahma, E. A. Terray, M. A. Donelan, and S. A. Kitaigorodskii, 1992: Observations of the enhancement of kinetic energy dissipation beneath breaking wind waves. *Breaking Waves,* M. L. Banner and R. H. J. Grimshaw, Eds., Springer, 95–101.

Ekman, V. W., 1905: On the influence of the earth's rotation on ocean currents. *Ark. Mat., Astron. Fys.,* **2**(11).

Ellison, T. H., 1956: Atmospheric turbulence. *Surveys in Mechanics,* G. Batchelor and R. Davies, Eds., Cambridge University Press, 400–430.

Gargett, A. E., 1989: Ocean turbulence. *Ann. Rev. Fluid Mech.,* **21,** 419–451.

Gill, A. E., 1982: *Atmosphere–Ocean Dynamics.* Academic Press, 662 pp.

Hopfinger, E. J., and J.-A. Toly, 1976: Spatially decaying turbulence and its relation to mixing across density interfaces. *J. Fluid Mech.,* **78,** 155–175.

Jenkins, A. D., 1986: A theory for steady and variable wind- and wave-induced currents. *J. Phys. Oceanogr.,* **16,** 1370–1377.

——, 1987: Wind and wave induced currents in a rotating sea with depth-varying eddy viscosity. *J. Phys. Oceanogr.,* **17,** 938–951.

Jenter, H. L., and O. S. Madsen, 1989: Bottom stress in wind-driven depth-averaged coastal flows. *J. Phys. Oceanogr.,* **19,** 962–974.

Jones, I. S. F., 1985: Turbulence below wind waves. *The Ocean Surface,* Y. Toba and H. Mitsayashu, Eds., D. Reidel, 437–442.

Kitaigorodskii, S. A., 1961: On the possibility of theoretical calculation of vertical temperature profile in upper layer of the sea. *Bull. USSR Academy Sci., Geophys. Series,* **3,** 313–318.

——, M. A. Donelan, J. L. Lumley, and E. A. Terray, 1983: Wave turbulence interactions in the upper ocean. Part II: Statistical characteristics of wave and turbulent components of the random velocity field in the marine surface layer. *J. Phys. Oceanogr.,* **13,** 1988–1999.

Klein, P., and M. Coantic, 1981: A numerical study of turbulent processes in the marine upper layers. *J. Phys. Oceanogr.,* **11,** 849–863.

Kundu, K. P., 1980: A numerical investigation of mixed-layer dynamics. *J. Phys. Oceanogr.,* **10,** 220–236.

Lobocki, L., 1992: Mellor-Yamada simplified second-order closure models: Analysis and application of the generalized von Karman local similarity hypothesis. *Bound. Layer Meteor.,* **59,** 83–109.

Ly, L. N., 1986: Modeling the interaction between atmospheric and oceanic boundary layers, including a surface wave layer. *J. Phys. Oceanogr.,* **16,** 1430–1443.

——, 1990: Numerical studies of the surface-wave effects on the upper turbulent layer in the ocean. *Tellus,* **42,** 557–567.

Madsen, O. S., 1977: A realistic model of the wind-induced Ekman boundary layer. *J. Phys. Oceanogr.,* **7,** 248–255.

Mellor, G. L., and P. A. Durbin, 1974: The structure and dynamics of the ocean surface mixed layer. *J. Phys. Oceanogr.,* **5,** 718–728.

——, and T. Yamada, 1974: A hierarchy of turbulence closure models for planetary boundary layers. *J. Atmos. Sci.,* **31,** 1791–1806.

——, and ——, 1982: Development of a turbulence closure model for geophysical fluid problems. *Rev. Geophys. Space Phys.*, **20,** 851–875.

Osborn, T., D. M. Farmer, S. Vagle, S. A. Thorpe, and M. Cure, 1992: Measurements of bubble plumes and turbulence from a submarine. *Atmos.–Ocean*, **30,** 419–440.

Phillips, O. M., 1977a: *Dynamics of the Upper Ocean.* 2nd ed., Cambridge University Press, 336 pp.

——, 1977b: The sea surface. *Modelling and Prediction of the Upper Layers of the Ocean,* E. B. Kraus, Ed., Pergamon, 229–237.

——, 1985: Spectral and statistical properties of the equilibrium range in wind-generated gravity waves. *J. Fluid Mech.*, **156,** 505–531.

Prandtl, L., 1952: *Essentials of Fluid Mechanics.* Blackie and Sons, 452 pp.

Richman, J. G., R. A. de Szoeke, and R. E. Davis, 1987: Measurements of near-surface shear in the ocean. *J. Geophys. Res.*, **92,** 2851–2858.

Rodi, W., 1987: Examples of calculation methods for flow and mixing in stratified fluids. *J. Geophys. Res.*, **92,** 5305–5328.

Shemdin, O. H., 1972: Wind-generated current and phase speed of wind waves. *J. Phys. Oceanogr.*, **2,** 411–419.

——, 1973: Modelling of wind-induced currents. *J. Hydraul. Res.*, **11,** 281–297.

Thompson, S. M., and J. S. Turner, 1975: Mixing across an interface due to turbulence generated by an oscillating grid. *J. Fluid Mech.*, **67,** 349–368.

Thorpe, S. A., 1984: On the determination of K_v in the near-surface ocean from acoustic measurements of bubbles. *J. Phys. Oceanogr.*, **14,** 855–863.

——, 1992: Bubble clouds and the dynamics of the upper ocean. *Quart. J. Roy. Meteor. Soc.*, **118,** 1–22.

——, 1993: Energy loss by breaking waves. *J. Phys. Oceanogr.*, **23,** 2498–2502.

Wang, D.-P., D. Chen, and T. J. Sherwin, 1990: Coupling between mixing and advection in a shallow sea front. *Contin. Shelf Res.*, **10,** 123–136.

Weber, J. E., 1981: Ekman currents and mixing due to surface gravity waves. *J. Phys. Oceanogr.*, **11,** 1431–1435.

——, 1983: Steady wind- and wave-induced currents in the open ocean. *J. Phys. Oceanogr.*, **13,** 524–530.

——, and A. Melson, 1993a: Transient ocean currents induced by wind and growing waves. *J. Phys. Oceanogr.*, **23,** 193–206.

——, and ——, 1993b: Volume flux induced by wind and waves in a saturated sea. *J. Geophys. Res.*, **98,** 4739–4745.

Wu, J., 1975: Wind-induced drift currents. *J. Fluid Mech.*, **68,** 49–70.

——, 1983: Sea-surface drift currents induced by wind and waves. *J. Phys. Oceanogr.*, **13,** 1441–1451.